Available online at www.sciencedirect.com
ScienceDirect
Physics Procedia 5 (2010) 177–186
Physics Procedia
www.elsevier.com/locate/procedia

LANE 2010

# Reflected Laser Radiation - Relevance for Laser Safety?

M. F. Zaeh[a], S. Braunreuther[a]*, R. Daub[a], T. Stadler[a]

[a]*Institute for Machine Tools and Industrial Management*
*Technische Universitaet Muenchen, 85747 Garching, Germany*

**Abstract**

Safety is compulsory in today's production lines. Those lines often use laser material processing applications. The highest risk for the operator or a bystander of a laser application is the exposure to the direct beam. With the present laser beam intensities, an accident at least causes sudden blindness or severe burns. Even if the process works correctly, which means the beam is always oriented towards the workpiece, the scattered and reflected parts of the laser beam still can be powerful enough to cause serious harm. The state-of-the-art safety measures are passive laser safety cabins around the application. Because of the high intensities and the low beam divergence of the highly brilliant laser beam sources, they cannot guarantee a safe use of these laser applications. An option is to use active laser safety barriers that react to an impinging laser beam on its surface.
A new approach to guarantee laser safety is to monitor the system and watch for incidents, to ensure that the laser spot never reaches the safety barrier. Assuming that accidents with the direct laser beam cannot occur, the passive safety measures still have to withstand the reflected laser radiation.
In this paper a theoretical model is presented with which the energy distribution in a hemisphere above a deep-welding-process can be calculated. The model was calibrated and validated with intensity measurements during a welding process. The results of the measurement can be used to develop a process-tailored safety cabin. Because of the increased mobility such a system increases the flexibility of the production cell. Furthermore, the costs for laser-safety may be decreased significantly.



*Keywords*: active and passive laser safety; reflected laser radiation; energy distribution; laser

## 1. Introduction

The application of high power laser systems for processes like welding or cutting is continuously increasing in industrial production lines. The most important characteristics in terms of production are: flexibility, accuracy and speed. The laser beam in such modern applications is very powerful, highly brilliant and invisible. Therefore, the direct and reflected laser radiation has a high risk potential. Conceivable claims are personal injuries like blindness, burns, long-tail claims, as well as material damage [1]. National and international laws [2, 3] demand safety for operators or bystanders next to machines in general. In case of laser applications, the standards and regulations [4-10] implement this demand for this category of machines. Conventional safety measures are housings for laser material processing centers. The protective effect is only provided by the laser safety walls of the housing. In the worst case, the laser beam can be oriented towards the protective wall. With long focal distances, which are

* Corresponding author. Tel.: +49-89-289-15559; fax: +49-89-289-15555.
*E-mail address*: stefan.braunreuther@iwb.tum.de.

1875-3892 
doi:10.1016/j.phpro.2010.08.135

available today, the maximum risk is a focused laser spot on the wall. Common laser safety cells are made of metal plates or stone walls. Usually the metal plates are about 2 mm thick and are arranged in a two- or more-layer design. The stone walls on the other hand are between 10 cm and 20 cm in thickness [1, 11]. The latest laser safety concepts use active guards in the wall that detect an impinging laser beam and shut down the system in that case. The "active" part in these systems is a sensor, monitoring light in the hollow-chamber or recognizing heat on the surface of the wall. Next generation laser safety concepts include the monitoring of the system status. Thus, a system shut down can be triggered by small irregularities, when the intended purpose of the application is not guaranteed anymore [1]. The purpose of such concepts is to avoid the exposure of the barrier to the direct laser beam. This can be achieved by watchdog systems which control the kinematics of the laser handling system. When a direct hit of the protection wall can be excluded, it just has to withstand the reflected and scattered radiation. For the development of a process monitoring system, Dietrich measured qualitative intensity values of the reflections of the laser process above the process zone [12]. In another work, Mueller determined the radiation from the process with a simulation model in order to improve the process quality, too. The data on which he calibrated the simulation were relative signal levels from sensors in front and in the back of the optical head [13]. In both works, the laser beam was inclined perpendicular and measurement points were few. Thus real intensity values of the reflected laser radiation depending on the process and laser beam inclination are unknown. For a better understanding of the behavior of reflected and scattered laser radiation of a deep welding process and to predetermine the load on laser safety walls, a theoretical model is presented in this paper. The proposed model was calibrated and compared with measurements of the reflected laser radiation of a deep welding process.

## 2. Theoretical model

The developed analytical model calculates the laser radiation intensities in a hemisphere above the process zone in dependence of the dominant process parameters like laser power $P_L$, inclination of the laser beam $\beta_i$ and material specific parameters like the absorption coefficient $a$. It is assumed, that the laser beam has a circular Gaussian intensity distribution. For a deep welding process, a certain threshold of laser intensity $I_{DW}$ is needed [14]. If the intensity is higher than $I_{DW}$, the metal is vaporized and a deep welding process with a keyhole formation is the result. The part of the laser beam with lower intensities than $I_{DW}$ does not penetrate the material, but causes heat conduction mode welding or heating on the plane surface of the material. The power of the laser beam is supposed to be partly absorbed or reflected differently by the material in the keyhole and on the plane surface. Therefore, the inclined laser power is divided into two parts: the laser power which forms the keyhole $P_K$ and the laser power which hits the plane surface $P_S$ [15]. The laser power, which is applied in the keyhole, can be calculated by integrating over the intensity distribution from the beam center to the spatial limitation of the keyhole $r_{DW}$, see Fig. 1.

$$P_K = 2\pi \int_0^{r_{DW}} \mathrm{r} \cdot I(r)_{Laser} \mathrm{d}r \qquad (1)$$

$P_K$ - power which forms the deep-welding-process, $I(r)_{Laser}$ - intensity distribution of the laser beam, $r_{DW}$ - limitation of the keyhole

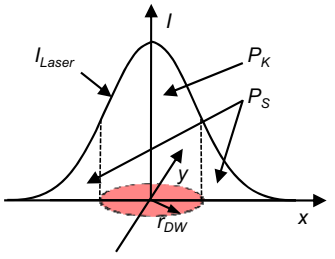


Fig. 1. Classification of the Gaussian intensity distribution on the workpiece coming from the laser

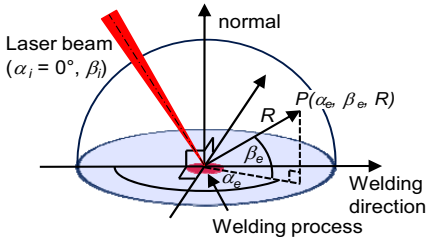


Fig. 2. Hemisphere above the welding process with polar coordinates

The power fragments $P_S$ and $P_K$ are partly reflected and can be divided into direct reflection ($P_{DR}$), keyhole reflection ($P_{KR}$) and scattered reflection ($P_{SR}$). They can be calculated using the following equations:

$$P_{DR} = (1 - a_S - s_S) \cdot P_S \quad (2)$$

$$P_{KR} = (1 - a_K - s_K) \cdot P_K \quad (3)$$

$$P_{SR} = s_S \cdot P_S + s_K \cdot P_K \quad (4)$$

$a_S$ - absorption coefficient of the plane surface, $a_K$ - absorption coefficient of the keyhole, $s_S$ - scattered reflection of the plane surface, $s_K$ - scattered reflection coefficient of the keyhole.

To calculate the energy distribution in a hemisphere above the keyhole, the intensity distributions of the three types of reflection have to be known as a function of space coordinates. In a spherical system, polar coordinates ($\alpha$, $\beta$ and $R$) are preferable, see Fig. 2.

As shown in Fig. 3 the reflected laser radiation propagates with different behaviors in this model. The coordinates of the emergent direct reflected (*DR*) beam ($\alpha_e$, $\beta_e$) are equal to ($\alpha_i$ + 180°, $\beta_i$). In this model, it is assumed that the inclined laser intensity $I_{Laser}$, which is higher than $I_{DW}$, forms a keyhole which has the same direction as the laser radiation. Therefore, the part of the laser beam which is reflected out of the keyhole (keyhole reflection - *KR*) has the opposite direction of the inclined laser radiation. A further presumption is that the emergent angle of the *KR* is the same as the angle of the inclined laser beam. In both cases, *DR* and *KR*, the beam qualities of the reflected laser beams are supposed to decrease. The scattered radiation (*SR*) is reflected into every direction.

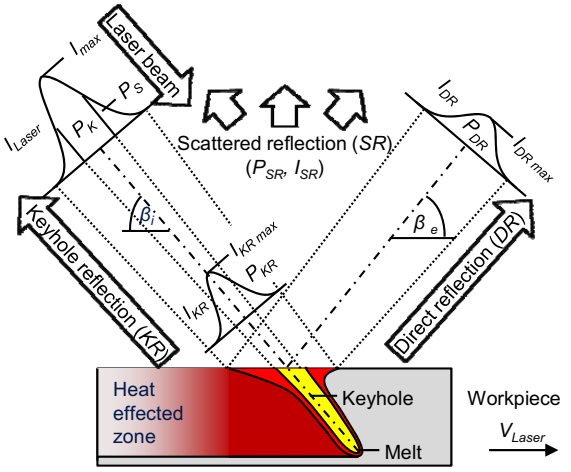


Fig. 3. The laser beam is assumed to be reflected directly (*DR*) on the plane surface, reflected from the keyhole (*KR*) and scattered (*SR*)

It is suggested to describe the *DR* and *KR* with a Gaussian distribution and the *SR* with the function of a Lambertian emitter [16]. Equation *(5)* describes a Gaussian intensity distribution.

$$I_{Gaussian} = \frac{2 \cdot P}{r^2 \cdot \pi} \cdot \exp(-2\frac{d^2}{r^2}) \quad (5)$$

$P$ - power, $r$ - radius of the laser beam using the 86% criterion, $d$ - distance to the center of the laser beam.

The intensity distribution of the scattered radiation is calculated by using the function of a Lambertian emitter.

$$I_{Lambertian} = \frac{P}{8 \cdot \pi^2 \cdot R^2} \cdot cos\beta \tag{6}$$

$R$ - radius of the hemisphere, $\beta$ - polar coordinate (compare Fig. 2).

In this theoretical model it is assumed that the focus of the laser beam is positioned on the surface of the material. The Gaussian distribution of $I_{DR}$ and $I_{KR}$ can be calculated by using the results of equations *(2)* and *(3)*, combined with equation *(5)*. The radius $r$ of the laser beam in a certain distance $R$ of the focus has to be calculated with the beam parameter product $BPP = \omega_0 \cdot \varphi$, where $\omega_0$ is the focal diameter with the 86% criterion and $\varphi$ the divergence angle of the Gaussian laser beam, see Fig. 4.

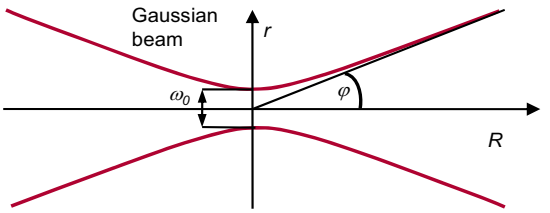


Fig. 4. Shape of a Gaussian beam. The distance $R$ from the focus is equal to the radius of the hemisphere for which the intensity distribution is calculated in this model

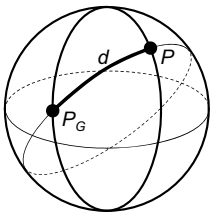


Fig. 5. The marked distance between point $P_G$ and $P$ is an orthodrome. It is the shortest connection between these two points on the sphere

Depending on the radius $R$ of the hemisphere $r$ is calculated individually for the *DR* and *KR* as:

$$r_{DR} = \tan\left(\frac{fq_{DR} \cdot BPP}{\omega_0}\right) \cdot R \tag{7}$$

$$r_{KR} = \tan\left(\frac{fq_{KR} \cdot BPP}{\omega_0}\right) \cdot R \tag{8}$$

$fq_{DR}$ - decrease of quality factor of the direct reflected laser beam, $fq_{SR}$ - decrease of quality factor of the laser beam reflected from the keyhole.

In equations *(7)* and *(8)* the variables $fq_{DR}$ and $fq_{KR}$ describe the expected decrease of quality of the *BPP* of the laser beam after the reflection on the workpiece. In the model the inclined laser beam always has the polar angles $\alpha_i = 0$ and $\beta_i$. This means that the center of the Gaussian distribution of $I_{KR}$ that is reflected from the keyhole has the coordinates ($\alpha_e = 0$, $\beta_e = \beta_i$, $R$). The center of the Gaussian distribution of the directly reflected intensity $I_{DR}$ has the coordinates ($\alpha_e = 180°$, $\beta_e = \beta_i$, $R$). Both intensities are shown in Fig. 3. As a simplification it is assumed, that the distance $d$ to the center of the Gaussian distribution from equation *(5)* is equal to the distance of the point of that center $P_G(\alpha_G, \beta_G, R)$ to the point $P(\alpha, \beta, R)$, which is valid as long as $R$ is at least one magnitude higher than $r$ ($R >> r$). With this assumption the distance $d$ is calculated for the *KR* and *DR* as $d_{KR}$ and $d_{DR}$ according to the calculation of an orthodrome [17] (see Fig. 5).

$$d_{KR} = \arccos(\sin(\beta_i) \cdot \sin(\beta) + \cos(\beta_i) \cdot \cos(\beta) \cdot \cos(\alpha)) \tag{9}$$

$$d_{DR} = \arccos(\sin(\beta_i + 90°) \cdot \sin(\beta) + \cos(\beta_i + 90°) \cdot \cos(\beta) \cdot \cos(180° - \alpha)) \tag{10}$$

The intensity distributions of *KR*, *DR* and *SR* can be calculated with equations *(1-10)* as:

$$I_{KR} = \frac{2 \cdot P_{KR}}{(\tan(\frac{fq \cdot BPP}{\omega_0})R)^2 \pi} \cdot \exp(-2\frac{(\arccos(\sin(\beta_i) \cdot \sin(\beta) + \cos(\beta_i) \cdot \cos(\beta) \cdot \cos(\alpha)))^2}{(\tan(\frac{fq_{KR} \cdot BPP}{\omega_0}) \cdot R)^2}) \quad (11)$$

$$I_{DR} = \frac{2 \cdot P_{DR}}{(\tan(\frac{fq \cdot BPP}{\omega_0})R)^2 \pi} \cdot \exp(-2\frac{(\arccos(\sin(\beta_i + 90°) \cdot \sin(\beta) + \cos(\beta_i + 90°) \cdot \cos(\beta) \cdot \cos(180° - \alpha)))^2}{(\tan(\frac{fq_{DR} \cdot BPP}{\omega_0}) \cdot R)^2}) \quad (12)$$

$$I_{SR} = \frac{P_{SR}}{8\pi^2 R^2} \cos\beta \quad (13)$$

The sum of equation *(11)*, *(12)* and *(13)* describes the intensity distribution of the reflected laser radiation of a deep welding process on a hemisphere above the process zone. It is described as a function of the polar coordinates $\alpha$, $\beta$ and *R*.

$$I_{total}(\alpha, \beta, R) = I_{SR} + I_{KR} + I_{DR} \quad (14)$$

The reflected intensity distributions $I_{SR}$, $I_{KR}$ and $I_{DR}$ contain several variables which are partly unknown. The variables which can be calculated, measured or defined are: $P_{SR}$, $P_{KR}$, $P_{DR}$, $\alpha$, $\beta$, *BPP*, $\omega_0$ and *R*. For other variables like the absorption and reflection coefficients $a_K$, $a_S$, $s_K$ and $s_S$ from equations *(2)*, *(3)* and *(4)* a possible value range is known from literature [18]. The value ranges of these variables together with the completely unknown values of the decrease of quality factors $f_{qDR}$, $f_{qKR}$ and the spatial limitation of the keyhole $r_{DW}$ will be used to calibrate the model with the measured intensity distribution in section 4.

## 3. Experimental setup

### *3.1. Optical measurement device and experimental procedure*

For the verification of the presented model, welding experiments were conducted. The experiments were done with a multi mode fiber laser with a maximum laser power of $P_L = 8$ kW. The focal length *f* of the optical head was 450 mm. The laser was positioned by a robot as shown in Fig. 6. The laser beam had a beam parameter product of *BPP* = 7.4 mm·mrad, a wavelength of $\lambda = 1070$ nm, a focal diameter of $d_f = 600$ µm and a Rayleigh length of $z_R = 11.7$ mm. The laser focus was positioned on the surface of a 3 mm thick stainless steel metal sheet (X6CrNiTi18-10), which was fixed on a linear axis. The axis was used to move the workpiece with a welding velocity of $v_{weld} = 6$ m/min. During the welding process the vapor was exhausted. The reflected and scattered radiation from the process zone was detected with a radiation-analyzer. This radiation-analyzer (Fig. 6) is composed of 15 measurement modules, mounted on a semicircle arc with a radius of 125 mm, which defines the radius *R* of the hemisphere. Each module consists of a defined aperture with a diameter of 0.5 mm in front of a silicium photo diode with a daylight filter, blocking wavelengths up to 780 nm. The optical axes of the modules are oriented to the center of the arc. Between every measurement run, the radiation-analyzer can be rotated around its axis, which is positioned perpendicular to the workpiece. Hereby, the reflected laser radiation in the hemisphere can be measured stepwise in several measurement runs. The hemisphere was measured for laser beam inclination angles $\beta_i$ of 50°, 60° and 70°. Every angle was measured for the laser power $P_L = 4$ kW, 5 kW, 6 kW and 7 kW.

### *3.2. Calibration and positioning of the radiation-analyzer*

Each of the measurement modules needed to be calibrated. Therefore, the laser beam was defocused to an intensity of about 2 W/cm² and oriented towards a calibrated reference sensor (PD 300-3W with filter, Ophir), with which the intensity was measured. After the calibration the reference sensor was replaced by a measurement module. The correlation between the measured intensity by the calibrated sensor and the corresponding current level of the measurement module resulted in a conversion factor. This factor was used to calculate the intensity from the measured current signal of the measurement module. The radiation-analyzer is equipped with two laser pointers irradiating towards the combustion point of the arc, see Fig. 6. With the help of those laser pointers, the center of the

radiation-analyzer was positioned at the focal point of the laser beam. The radiation-analyzer was mounted on the robot with an adjustable device. Because of the defined aperture of the measurement modules the photodiodes can only "see" the process zone. A servo drive in the vertical axis between the mounting device and the radiation-analyzer rotated the arc incrementally in steps of 15°. A rotation of 180° would describe a complete hemisphere above the laser welding process. Because of spatial limitations due to the inclined laser beam, the extreme positions could not be realized, so that the hemisphere is not fully covered.

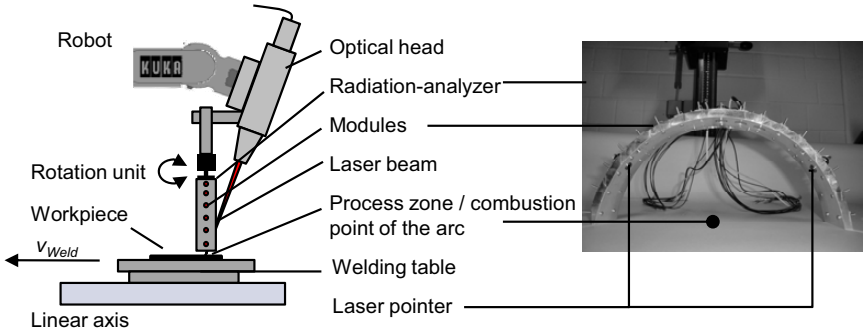


Fig. 6. An 8 kW fiber laser welds the workpiece, which is moved by a linear axis. During the process the radiation-analyzer, which consists of 15 measurement modules, measures the reflected laser radiation in a hemisphere above the process zone. The measurement element in every module is a photodiode with a daylight filter blocking the process radiation

### *3.3. Error estimation*

The values, which are measured with the radiation-analyzer, are associated by measurement failures. These failures contain a systematic and a random error. The errors which were taken into account are listed in Table 1. It can be seen that the biggest measurement failures results from the unstable measurement conditions. The measured values are strongly influenced by the welding vapor and instabilities of the welding process.

Table 1. Values for the error estimation

| Error source | Error Type | Value / % |
|---|---|---|
| A/D conversion | Systematic error | ± 0.0184 |
| Measured reproducibility | Random error | ± 21 |
| Stability of the laser power | Random error | ± 2 |
| Measurement failure of the reference sensor | Random error | ± 7 |
| Positioning failure of the reference sensor | Random error | ± 3 |
| Measurement failure of the measurement module (estimation) | Random error | ± 10 |
| Positioning failure of the measurement module (estimation) | Random error | ± 3 |

The total measurement failure is the sum of the systematic and the random errors [19]:

$$\Delta f = \Delta f_s + \Delta f_r \tag{15}$$

$\Delta f$ - total measurement failures, $\Delta f_s$ - sum of the systematic errors, $\Delta f_r$ - sum of the random errors.

$\Delta f_s$ is:

$$\Delta f_s(x_1, x_2, ...) = \sum_{i=1}^{N} \frac{df}{dx_i} \Delta x_i \quad (16)$$

$x_i$ - parameter, $\Delta x_i$ - root mean square deviation of the parameter $x_i$, $N$ - number of parameters.

$\Delta f_r$ is:

$$\Delta f_r(x_1, x_2, ...) = \sqrt{\sum_{i=1}^{N} (\frac{df}{dx_i})^2 \Delta x_i^2} \quad (17)$$

$x_i$ - parameter, $\Delta x_i$ - root mean square deviation of the parameter $x_i$, $N$ - number of parameters.

With equation *(15)*, *(16)*, *(17)* and the values from Table 1 the total error can be estimated as:

$$\Delta f = 24.76\% \quad (18)$$

## 4. Empirical results and calibration of the theoretical model

### *4.1. Measured intensity*

Fig. 7 (left) shows the measured intensity distribution in the hemisphere at a radius of $R = 125$ mm above the welding process with $v_{weld} = 6$ m/min and a laser power of $P_L = 7$ kW. The inclination angle of the laser beam is $\beta_i = 50°$. The diagram represents a view from the top onto the laser-welding-process. The inclined laser beam penetrates the hemisphere at the coordinates $\alpha = 0°$ and $\beta = 50°$. In this area the *KR* results in intensities between 2.5 W/cm² and 2.75 W/cm². The direct reflection is depicted around the coordinates $\alpha = 180°$ and $\beta = 50°$ with intensities up to 3 W/cm².

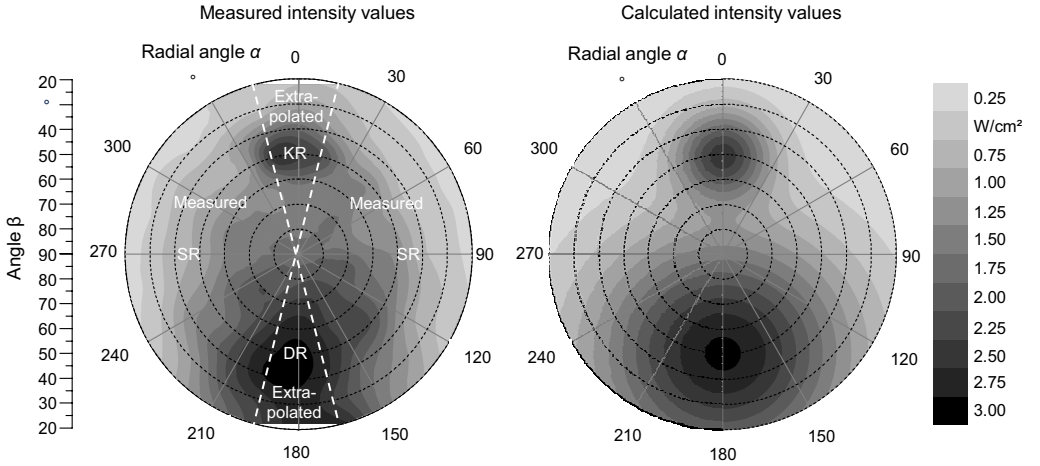


Fig. 7. Measured (left diagram) and calculated (right diagram) intensity radiation in a distance of $R = 125$ mm from the process; laser power $P_L = 7$ kW; $v_{weld} = 6$ m/min; laser beam inclination $\beta_i = 50°$

The *SR* is superimposed onto the whole surface of the hemisphere. On both sides it decreases with smaller angles of $\beta$. Because of geometrical boundary conditions, not the whole hemisphere could be measured. In Fig. 7 (left) the values for the radial angle $\alpha = 345°$ to 15° and the complement on the other side, $\alpha = 165°$ to 195° were not measured. Intensity values in these areas of the hemisphere were extrapolated. The theoretical model of the reflected laser radiation was calibrated using the measured data at $\beta_i = 50°$ and $P_L = 7$ kW. The calibration was done by varying the unknown parameters in the theoretical model. The used values of the parameters are given in Table 2. A plot of the calculated laser radiation intensities is depicted in the right diagram of Fig. 7. The characteristics and the values of the measured and the calculated intensities are in good agreement.

Table 2. Parameters of the calibrated theoretical model

| Parameter | Symbol | Value | Data Source |
|---|---|---|---|
| Absorption coefficient on a plane surface | $a_S$ | 0.4 | measured |
| Absorption coefficient of the keyhole | $a_K$ | 0.975 | calibrated |
| Spatial limitation of the keyhole | $r_{DW}$ | 0.12 mm | calibrated |
| Coefficient of the scattered direct reflection | $s_S$ | 0.3 | measured |
| Coefficient of the scattered keyhole reflection | $s_K$ | 0 | calibrated |
| Decrease of quality direct reflection | $fq_{DR}$ | 42 | calibrated |
| Decrease of quality keyhole reflection | $fq_{KR}$ | 20 | calibrated |

### *4.2. Characteristics of keyhole radiation and direct radiation*

The areas in Fig. 7 with the highest intensity values on the hemisphere are those with the *KR* and the *DR*. Both central axes of these reflections are in a plane. On the one half of the plane, the radial angle $\alpha$ is 0° (half-plane of *KR*), on the other half $\alpha$ is 180° (half-plane of *DR*). The angle $\beta$ varies from 90°, meaning perpendicular to the workpiece, to 0° on both sides. Like depicted in Fig. 7 (left), the intensity values in this plane are extrapolated out from their neighboring values. The diagrams in Fig. 8 show the nearest measured values at $\alpha_e = 15°$, $\alpha_e = 195°$ respectively (Fig. 7, left diagram, dashed line) of the laser intensity for a laser beam inclination of $\beta_i = 50°$, at a laser power of $P_L = 5$ kW (left) and $P_L = 7$ kW (right).

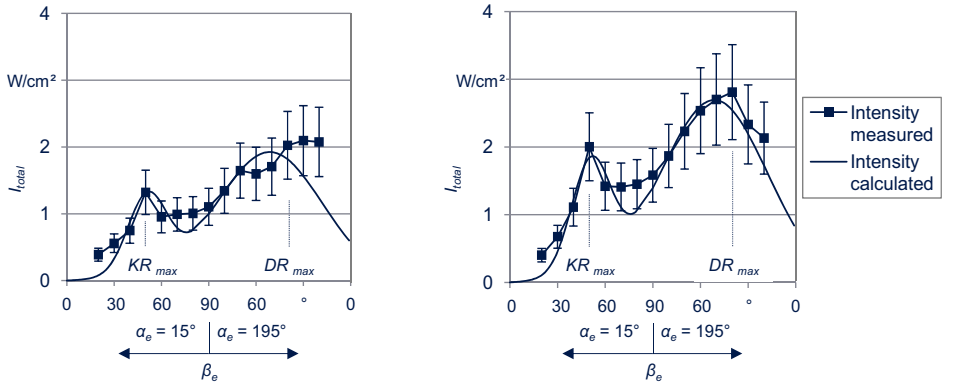


Fig. 8. Measured and calculated profiles of the reflected laser radiation intensity on the hemisphere in the *KR* and the *DR* plane; $\beta_i = 50°$; $P_L = 5$ kW (left) and $P_L = 7$kW (right), $v_{weld} = 6$ m/min

The error bars represent the measurement failures (see section 3.3). The maxima of the *KR* and of the *DR* are visible in the peaks of the graphs. For *KR*, the peak can be found at $\alpha_e$ between 345° and 15° and $\beta_e = 50°$, which represents the central axis of the reflected laser beam. The maximum of *DR* is located at the coordinates $\alpha_e$ between

165° and 195° and $\beta_e = 50°$. Both diagrams are complemented with the calculated intensity distribution, according to the theoretical model.

### *4.3. Directions of reflected laser radiation*

As already mentioned, the most intense areas of the reflected laser radiation on the hemisphere are the keyhole reflection and the direct reflection. To avoid danger, it is necessary to know their position on the hemisphere. For that reason, Fig. 9 shows the angle of the central axis of the keyhole reflection $\beta_{KR}$ and of the direct reflection $\beta_{DR}$ in dependence of the inclination angle of the laser beam. In both cases, the assumption which was made in section 2, that the angle $\beta_i$ of the inclined laser beam and the angles $\beta_{KR}$ and $\beta_{DR}$ of the *KR* and the *DR* are equal, is confirmed.

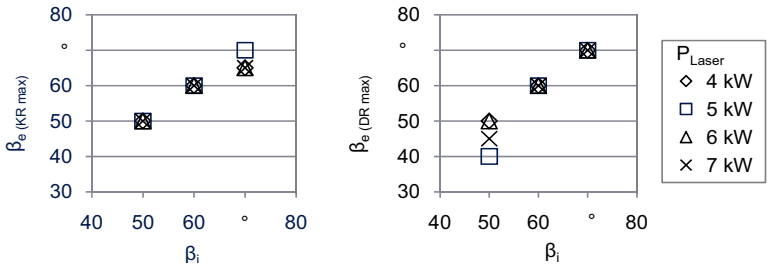


Fig. 9. Inclination angles of *KR* and *DR* depending on inclined laser beam and laser power

## 5. Relevance for laser safety

For laser safety concepts it is essential to know the highest possible laser radiation intensity and its location [20]. In conventional laser applications, this intensity can occur by an exposure to the direct laser beam. If the laser system is completely monitored, meaning the system is always in accordance with the reference values, there is no danger from the direct laser beam [1]. In this case, the reflected laser radiation represents an undetermined source of danger. For the deep-welding-processes in this publication, the maximum reflected laser intensities on a hemisphere with a radius of 125 mm were in the magnitude of about 3 W/cm². However, it should be considered that those values are extrapolated since the measurement setup did not allow to measure in the whole area of the *KR* and *DR*. The presented model allows the calculation of the values of the reflected laser radiation of the considered deep-welding-process in dependence of the distance to the process area.

The maximum intensity limit for the human skin, irradiated with a wavelength of $\lambda = 1070$ nm for a exposure time of $t = 10$ s is 1 W/cm² [10]. The tolerable intensity for the irradiation of the human eye only is 5 mW/cm² [10].

**The reflected parts of the laser radiation have to be considered. They are relevant for laser safety!**

To avoid serious harm, laser safety measures are required. Passive laser safety barriers, for example made from steel, detain laser radiation up to about 120 W/cm² [21]. According to the standards and regulations [22] laser safety glasses could be conceivable for those reflected intensities, too.

## 6. Summary and outlook

In this publication, a theoretical model for the calculation of laser intensities in a hemisphere around a laser-deep-welding process was presented. To validate this model, welding experiments were conducted with different laser powers and laser beam inclinations. During each welding process, a calibrated radiation-analyzer was used to measure the reflected parts of the laser beam in a hemisphere around the process. In this way the intensity values were associated with positions relative to the process zone. Those data were used to calibrate the theoretical model.

In terms of laser safety, this model is a powerful tool to estimate the maximum possible laser intensity for a given laser process and a given distance to this process. Since the behavior of the reflection is suggested to depend strongly on the material and the surface roughness of the workpiece the measured intensity values and the presented

theoretical model can not be generalized, yet. Thus, the reflected laser radiation can be more dangerous for other process configurations.

To get a more precise and general model of the reflected laser radiation of a deep-welding-process the radiation-analyzer has to be improved so that the whole hemisphere can be measured. The effect of the surface roughness and the material of the workpiece on the behavior of the reflectance factor have to be investigated as well as different welding speeds and keyhole shapes. The aim of these tests is to build up a large database that allows the improvement of the theoretical model of the reflected laser radiation for that process. Parallel to the improvement of the deep-welding-process-reflection-model other processes with relevance for industrial applications, like laser-cutting, have to be investigated.

## Acknowledgements

The presented results were developed within a project on concepts to support the laser safety for highly brilliant laser beam sources, supported by the foundation “Arbeitsgemeinschaft industrieller Forschungsvereinigungen - Otto von Guericke e.V.” (AIF) and “Deutscher Verband fuer Schweißen und verwandte Verfahren e.V.” (DVS).

## References

1. M. F. Zaeh, S. Braunreuther, S. Huber, F. Oefele and A. Trautmann, Systematic Development of Safe High Performance Laser Applications - Knowing the Limits of Conventional Systems, ICALEO, LIA, Orlando, 2009, Paper 905.
2. Bundesrepublik Deutschland, Gesetz ueber technische Arbeitsmittel und Verbraucherprodukte, 2004.
3. Europaeisches Parlament, Richtlinie 2006/42/EG, 2006.
4. VDE, EN 50825-1: Sicherheit von Lasereinrichtungen - Part 1, Klassifizierung von Anlagen und Anforderungen (IEC 50825-1:2007), Beuth, Berlin, 2008.
5. VDE, EN 50825-2: Sicherheit von Laser-Einrichtungen - Part 2, Sicherheit von Lichtwellenleiter-Kommunikationssystemen (LWLKS) (IEC 50825-2:2004 + A1:2006), Beuth, Berlin 2007.
6. VDE, EN 50825-4: Sicherheit von Lasereinrichtungen - Part 4, Laserschutzwaende - neuer Anhang G ueber Strahlfuehrungssysteme (IEC 76/362/CDV:2007), Beuth, Berlin, 2007.
7. Deutsches Institut fuer Normung e. V., DIN EN ISO 11553-1: Sicherheit von Maschinen – Laserbearbeitungsmaschinen - Part 1, Allgemeine Sicherheitsanforderungen, Beuth, Berlin, 2008.
8. Deutsches Institut fuer Normung e. V., DIN EN ISO 11553-2: Laserbearbeitungsmaschinen – Part 2, Sicherheitsanforderungen an handgefuehrte Laserbearbeitungsgeraete, Beuth, Berlin, 2008.
9. Deutsches Institut fuer Normung e. V., DIN EN ISO 11553-3: Sicherheit von Maschinen – Laserbearbeitungsmaschinen – Part 3, Sicherheitsanforderungen zur Laermminderung und Geraeuschmessverfahren fuer Laserbearbeitungsmaschinen und handgefuehrte Laserbearbeitungsgeraete sowie zugehoerige Hilfsmittel, Beuth, Berlin, 2008.
10. BGETE, BGV B2 - Unfallverhütungsvorschrift Laserstrahlung, Berufsgenossenschaft der Feinmechanik und Elektrotechnik, Koeln, 2007.
11. S. Braunreuther, Anlagensicherheitskonzepte fuer Hochleistungslaser der neuesten Generation, Sicherheit bei der Materialbearbeitung mit Laserstrahlung, BGIA, Hennef, 2009, pp. 181-186.
12. S. Dietrich, Sensoriken zur Schwerpunktslagebestimmung der optischen Prozessemissionen beim Laserstrahltiefschweißen, Meisenbach, Bamberg, 2009.
13. M. G. Mueller, Prozessueberwachung beim Laserstrahlschweißen durch Auswertung der reflektierten Leistung, Utz, Muenchen, 2002.
14. R. Poprawe, Lasertechnik fuer die Fertigung, Springer, Berlin, 2005.
15. M. Beck, Modellierung des Lasertiefschweißens, Teubner, Stuttgart, 1996.
16. C. Gerthsen and D. Meschede, Gerthsen Physik, 22nd ed., Springer, Berlin, 2004.
17. J. Meeus, Astronomical algorithms. 2nd ed., Willmann-Bell, Richmond, 1998.
18. R. Poprawe, D. Baeuerle, H. Landolt, R. Boernstein, W. Martienssen and O. Madelung, Numerical data and functional relationships in science and technology, Springer, Berlin, 2004.
19. F. Adunka, Meßunsicherheiten. 2nd ed.,Vulkan, Essen, 2000.
20. M. Alunovic and E. W. Kreutz, Abschirmung an Laserarbeitsplaetzen, Wirtschaftsverlag, Bremerhaven, 1996.
21. J. Franek and E. M. Heberer, Requirements for Laser Guards Femtosecond Lasers in Comparison to usual High Power Lasers, ILSC, LIA, San Francisco, 2007, Paper 907.
22. BGETF, Auswahl und Benutzung von Laser-Schutz und Justierbrillen, Berufsgenossenschaft Textil Feinmechanik, Koeln, 2007.